International Journal on Interactive Design and Manufacturing (IJIDeM)
https://doi.org/10.1007/s12008-023-01452-z

ORIGINAL PAPER

Design and numerical analysis of tensile deformation and fracture properties of induction hardened inconel 718 superalloy for gas turbine applications

Mohammed Asif Kattimani[1] · P R Venkatesh[1] · Habib Masum[2] · Mahantesh M Math[1] · Vikram N Bahadurdesai[3] · Syed Mustafkhadri[4] · C Durga Prasad[5] · Hitesh Vasudev[6]

Received: 27 May 2023 / Accepted: 4 July 2023

Abstract

This study examines the design and numerical analysis of induction hardened of Inconel 718 superalloys on the tensile properties. The two tensile specimens (IHT1 & IHT2)'s outside surfaces are heated to temperatures of 850 and 1000 °C. The heated samples are then quenched in oil. The samples are evaluated utilizing a 250kN capacity servo hydraulic universal test at ambient temperature and an enhanced temperature of 800 °C. At both room temperature and a raised temperature of 800 °C, the metrics yield strength (YS), ultimate tensile strength (UTS), and elongation of induction hardened sample have risen. Induction-hardened materials have better mechanical characteristics than non-induction-hardened samples, according to numerical results from ANSYS Workbench that are corroborated with experimental data. The results of the tensile test's cracked surfaces under a scanning electron microscope (SEM) show that the presence of shallow dimple structure at 800 °C caused transgranular cleavage and intergranular dimple rupture as the modes of failure.

Keywords Induction hardening · Inconel 718 · Microstructure · Oil quenched · ANSYS · SEM

1 Introduction

Combustion chambers, aircraft turbine discs, shafts, fasteners, and guiding vanes are just a few examples of crucial components made from Inconel 718 (IN718) that are often utilised in the aerospace industry [1, 2]. It possesses strong corrosion resistance, great oxidation resistance at high temperatures, and excellent cycle fatigue resistance [3]. The tensile strength of it is likewise quite high. The IN718 alloy is a typical face-centered cubic (FCC) nickel-based superalloy as a result of precipitate strengthening. The modest amounts of metastable γ' phase (Ni3Nb-based D022 structure), spherical γ'' phase (Ni3Al-based L12 structure), and carbides that are present in Inconel 718 are what give it its high thermal strength [4–7]. The quantity and size of the γ' phase γ'' that exhibits significant coherence with the matrix will have a direct impact on the alloy's overall mechanical properties. The incoherent equilibrium phase (Ni3Nb-based D0a structure), which may stably remain at increased temperatures and diminish the alloy's strength, is unstable and prone to shift into the "phase when exposed to prolonged high temperatures or during heat treatment.

✉ C Durga Prasad
durgaprasi71@gmail.com

✉ Hitesh Vasudev
hitesh.24804@lpu.co.in

1 Department of Mechanical Engineering, RVCE, Bengaluru, India

2 Department of Mechanical Engineering, Ghani khan Choudhury Institute of Engineering and Technology, Narayanpur, Malda, West Bengal, India

3 Department of Industrial Engineering & Management RVCE, Bengaluru, India

4 Department of Mechanical Engineering, Global Institute of Engineering and Technology, Hyderabad, India

5 Department of Mechanical Engineering, RV Institute of Technology and Management, Bengaluru, India

6 Lovely Professional University, Phagwara, India

Published online: 12 July 2023

As a structural element of an aero-engine, the IN718 alloy experiences continual high temperatures and high stresses, which change the microstructure of the alloy. The mechanical characteristics of materials are directly influenced by the evolution of the microstructure [8].To comprehend the fracture process of IN718 alloy under identical service circumstances, it is required to investigate the dynamic relationship between the evolution of the microstructure and change in the mechanical characteristics of the alloy. Numerous studies have looked at the structure-property correlations and deformation behaviours of the alloy IN718 at various temperatures. Ex-situ tensile testing was used by Wang et al. [9] to examine the hot deformation behaviours of the IN718 alloy at high temperatures between 950 and 1050 °C. They discovered that dynamic recrystallization is responsible for the flow oscillations in stress at lower strain rates. Liu et al. [10] evaluated the effect of grain size on the fracture behaviour in uniaxial tensile tests on IN718 sheets carried out at room temperature and interpreted the fracture behaviour in terms of the influence of the microstructure, but they failed to consider the effect of tensile temperature. Based on the post-mortem observation of fracture morphology by SEM, Zhao et al. [11] proposed a two-step fracture process after examining the impacts of grain size and strain rate on the fracture behaviours of IN718 thin sheets. Lin et al. [12] investigated the effects of deformation temperature and strain rate on the fracture morphology of IN718 by performing heat-treated hot uniaxial tensile tests at temperatures between 920 and 1040 °C and strain rates between 0.001 and 0.01 s-1.They found that the temperature, strain, and strain rate of the deformation had a substantial impact on the flow behaviours.

Even though several of the IN718 alloy's tensile deformation behaviours at high temperature were investigated, the research are mostly conducted without induction hardening tensile testing. The bulk of fracture mechanisms are deduced by fractographic analysis from hypothesised fracture processes [13]. It is important to compare the microstructure evolution and the complete fracture process during tensile testing at room temperature and higher temperature with induction hardening in order to fully understand the effects of deformation temperature on the fracture mechanism of IN718 alloy. Uniaxial tensile tests are employed in this studies to compare the mechanical properties of non-induction hardened Inconel 718 alloy with induction hardened Inconel 718 alloy at room temperature (RT) and 800 °C. The fracture initiation and propagation mechanisms are seen in the SEM after tensile testing. In light of the experimental results, the effects of induction hardening on microstructure, hardness, and mechanical properties are examined. The experimental results are only valid at a particular temperature of 800 °C. Understanding the relationship between structure and properties as well as the superalloy's fracture process at various temperatures would be beneficial.

2 Material and methods

2.1 Methodology

Overall methodology of the research undertaken is shown in Fig. 1. A thorough review of the literature revealed that high temperature tensile test of Inconel 718 superalloys have rarely been quantified and characterized. A specimen of commercial Inconel 718 alloy have taken and subjected to induction hardening and details study of mechanical properties of treated superalloys with untreated one as point of comparison under tensile tests at room temperature and 800 °C have been done.

2.2 Experimental procedure

The testing specimens are induction hardened using an industrial induction hardening machine of power density 26–40 kW, frequency 7.8 Hz, voltage 240 V, current 30 amps and coil testing specimen distance is 3 mm. The Vickers hardness test is carried out for inconel 718 untreated and induction hardened specimens at (Jyothi Specto Analysis, Hyderabad-India) with a 5kgf test load, using MVN-50PC 115–0618 equipment. The test is conducted according to standard procedures, using an indenter on a square diamond pyramid with the plane angle of 136°.

The following procedures are carried out in order to capture a good microstructure: (1) grinding (2) polishing (3) etching. Three stepsd of grinding with Silicon Carbide (SiC) emery paper at SiC 500 (30 m), SiC 2000 (10 m), and SiC 4000 (5–6 m) are carried out for 3–5 min. The specimens are polished by placing them on a disc polishing machine that rotates in an anti-clockwise circular motion for 15 min, 1 Mol (cotton and nylon cloth plate), 0.25 Nap (fibre plate), Non-crystallizing colloidal Silica polishing suspension on Chem cloth for 5 min, and water polishing for 30 s on another Chem cloth. Hydrochloric acid (HCl) and oxalic acid (H2C2O4) were mixed 50:50 to perform the etching. After the sample preparation process the microstructure of the specimen is investigated using scanning electron microscope (SEM) with a specifications of magnification of (TESCAN VEGA 3 SEM), Electron gun (Tungsten heated cathode), Resolution (3 nm at 30 kV / 2 nm at 30 kV) Magnification ($2\times - 1{,}000{,}000$x), Probe Current (1pA to 2 μ A).

For the uniaxial tensile test at room temperature (RT) in accordance with ASTM E8-21 standards, a servo hydraulic tensile testing machine setup (BISS, 250kN, UTM) is also used, while (BISS, 0-40T, AI UTM equipped with an

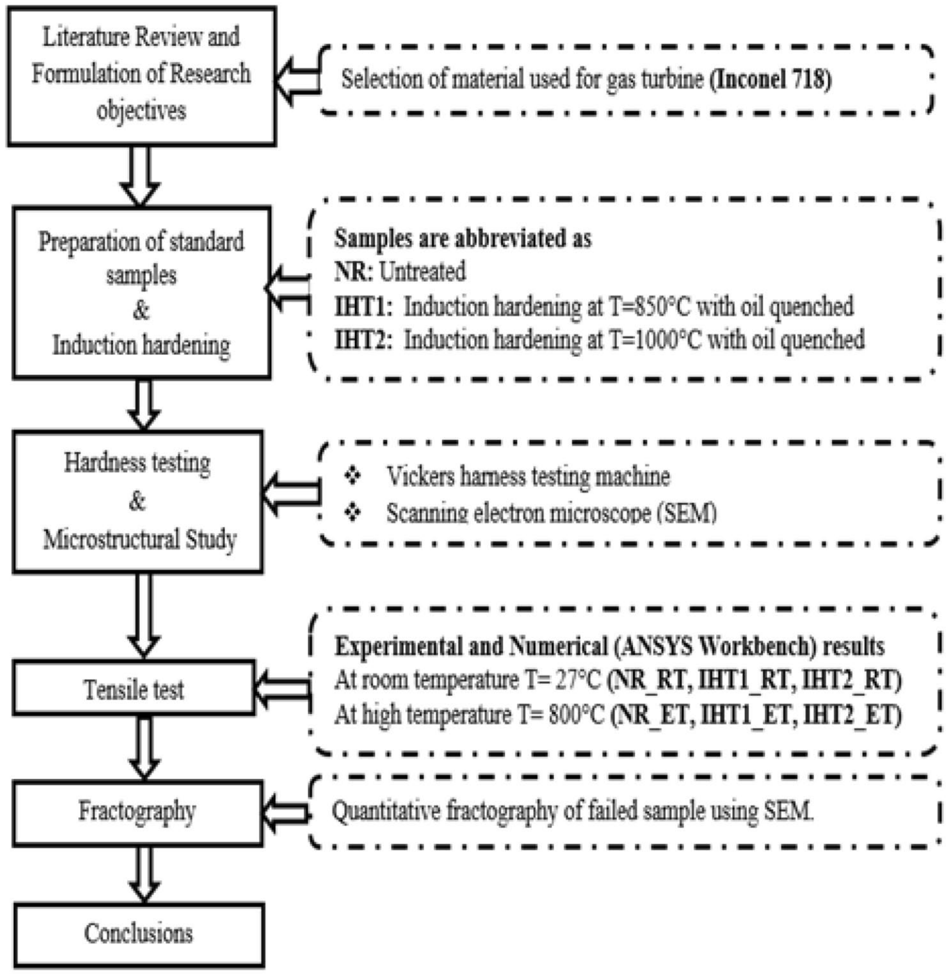

Fig. 1 Overall research methodology

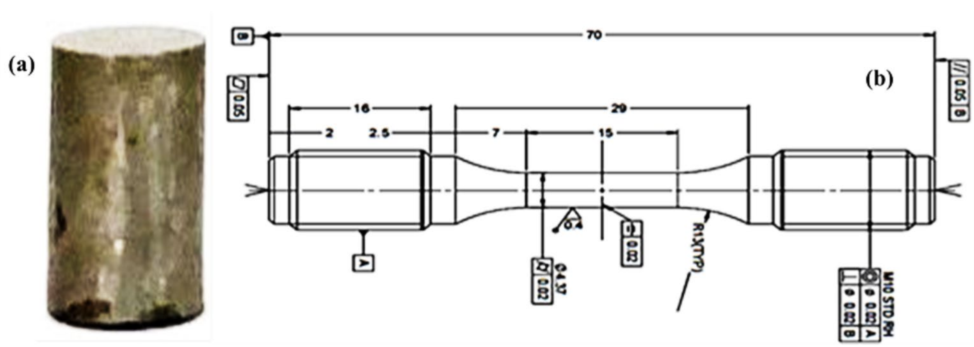

Fig. 2 **(a)** Microstructure and Hardensss test specimen **(b)** Tensile test specimen dimension

Environmental Test Chamber (ETU: chamber) is utilised for elevated temperature of 800 °C in accordance with ASTM E21-20 at the same strain rate of 0.0167 mm/sec. For each condition, the test is conducted three times, and the results of the elongation, yield strength, and ultimate tensile strength tests are presented as an average value of 0.2%. It would be beneficial to conduct elevated temperature (ET) tensile testing to compare the results to room temperature tests and to comprehend the static behaviour. The SEM at a voltage of 15 kV shows the crack initiation and propagation processes using the fracture surfaces of the failed specimen. For the quantitative evaluation of precipitates, the SEM is outfitted with Image Pro-Plus 6.0 software and energy dispersive spectrometry (EDS).

2.3 Specimen preparation

As seen in Fig. 2(a), three specimens with a diameter of 12.7 mm and a height of 50 mm were cut from a long Inconel 718 ingot.Table 1 lists the chemical makeup of Inconel

Table 1 Chemical composition of Inconel 718

COMP	Ni	Cr	Mn	Co	Mo	Si	Ti	Al	Fe	Nb
%	51.7	17.7	0.3	0.3	3.11	0.18	0.8	0.43	19.86	5.05

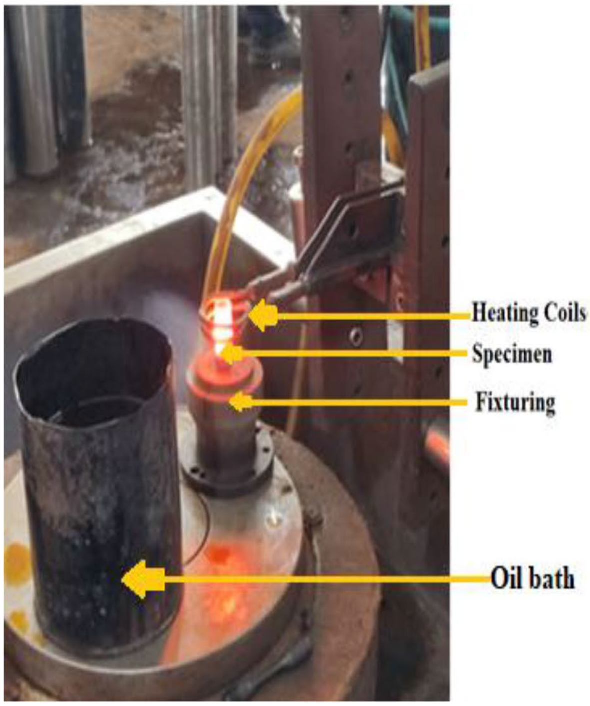

Fig. 3 Induction hardening of machined specimens **(a)** induction hardened at T = 850°C (IHT1) **(b)** Induction hardened at T = 1000°C IHT2

Fig. 4 Vicker Harness (HV) values of samples

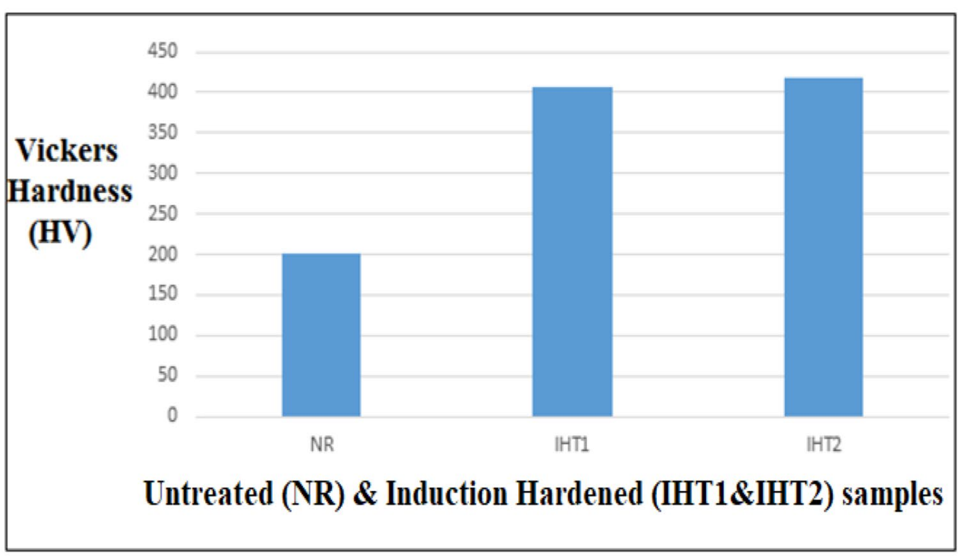

718 as determined by positive material identification (PMI) testing. The ASTM E468-08 (M10-standard) dimensions for the hourglass-shaped standard tensile test specimens are illustrated in Fig. 2(b).The specimens' exterior surfaces are

heated to two distinct temperatures 850 and 1000 °C for a total of 10 to 15 s each.The coil's alternating current causes the specimen to develop an induced magnetic field. The heated specimens are then cooled in oil as seen in Fig. 3. The untreated sample is designated as (NR), whereas specimens that were induction hardened at temperatures of 850 and 1000 °C are designated as IHT1 and IHT2, respectively.

3 Result and discussions

3.1 Hardness test

Figure 4 displays the average values for the three places where the measurements are taken. The average hardness values of untreated specimen is 200.33 HV whereas induction hardened specimen (IHT1 and IHT2) values are 407 HV and 417 HV respectively. In comparison to untreated (NR) and induction hardened at 850 °C (IHT1), the induction hardened sample at 1000 °C (IHT2) shows better hardness.

3.2 Microstructures

Figure 5 shows the high resolution SEM microstructures image of the untreated and induction hardened specimens. For the untreated superalloy, the grain size for a given location is smaller than that of the induction hardened (Fig. 5a). This indicates that during induction hardening, grain enlargement, has taken place. It is important to note that the applied induction hardening lead to uniformity in grain size and strengthening the grain boundaries by acting barriers to dislocation motion. Induction hardened at T = 850℃ (IHT1) superalloy's microstructure shows (Fig. 5b) evidence of grain size increment and presence of γ' distributed in the grain boundaries and NbC carbides have needle-like and blocky morphologies, respectively [14, 15]. In the induction hardened at T = 1000℃ (IHT2) it can be observed that the grains are equiaxed with the equal grain size. In addition, lamella-like twins formed and presence of two morphologies of γ'' and γ' polygonal-shaped particles embedded inside matrix (marked by yellow arrows) can be seen in (Fig. 5c), δ phase particles distributes in the grain boundaries which are confirmed to be (Nb, Ti) C carbides.

3.3 Tensile properties

An induction hardening-induced strengthening mechanism is used to explain the outcomes of stress and strain. Comparing Inconel 718 to a non-induction-hardened alloy, the yield strength has increased and the specific elongation has altered taking into account the elevated temperature (ET) of 800^0 C, the experimental value of ultimate tensile strength (UTS), yield stress (YS), elongation to fracture and reduction of cross section are tabulated in Table 2. A high elongation value implies good plasticity, and it is a key measure of a material's capacity for plastic deformation. It is clear that the specimen with the highest value of elongation is the one that is at room temperature (IHTT2_RT). The specimens NR_RT, IHT1_RT, and IHT2_RT have final gauge lengths of 22.84 mm, 24.01 mm, and 25.23 mm, respectively. And the respective elongations are 26.89%, 33.39%, and 40.17%. The presence of the γ'' and γ' phases

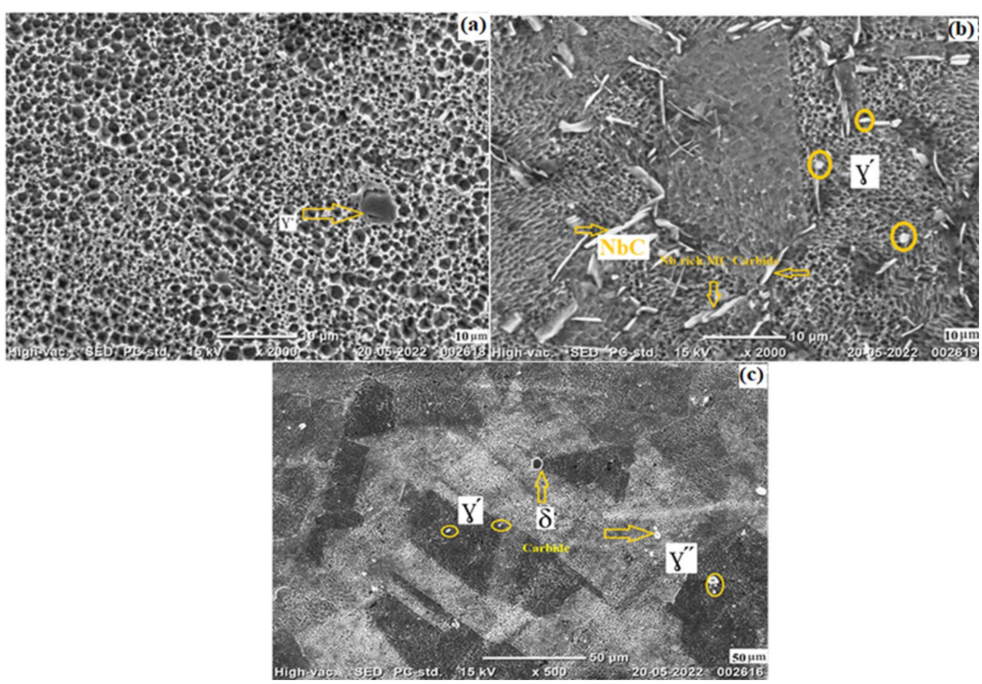

Fig. 5 High-resolution SEM Images of IN718 Samples **(a)** SEM image of untreated samples **(b)** SEM images of induction hardened at T = 850℃ (IHT1) (c) SEM images of induction hardened at T = 1000℃(IHT2)

Table 2 Tensile properties of untreated and induction hardened sample at room temperature and elevated temperature (800°C)

Testing Specimen	YS (MPa)	UTS (MPa)	Elongation (%)	Area reduction (%)	Final gauge length (mm)
NR_RT	790.51	964.79	26.89	64.00	22.84
NR_ET	667.98	737.02	6.11	80.0	19.10
IHT1_RT	959.53	1265.34	33.39	57.57	24.01
IHT1_ET	698.08	749.17	13.39	89.0	20.41
IHT2_RT	1177.96	1451.48	20.61	33.87	21.71
IHT2_ET	790.93	847.47	40.17	67.20	25.23

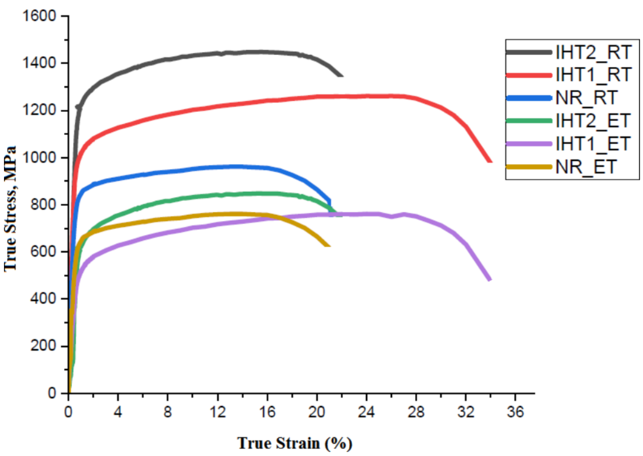

Fig. 6 Stress vs. Strain graph of IN718 of untreated and induction hardened samples at room temperature

demonstrates that the specimens plasticity grows while induction hardening proceeds. When comparing induction hardened test results obtained at elevated temperatures of 800 °C with those obtained at room temperature, it appears that elongation, yield strength, ultimate strength, and toughness are decreasing. This behaviour might be explained by the existence of δ phase particles. Figure 6 accompanying stress-strain graphs for the tested samples. It indicates that strength has slightly decreased in cases of elevated temperature when comparing the elevated temperature tensile strength for induction hardened superalloys with the room temperature tensile strength. It is evident that the specimens with induction hardening tensile stress-strain curves undergo three stages of deformation, typical all curves are elastic with uniform plastic. While parabolas in the tensile curves indicate consistent plastic deformation when the tension reaches the yield strength, straight lines in the early stages of deformation indicate elastic deformation. When the tension approaches the maximum tensile strength, necking, a non-uniform plastic deformation, occurs.

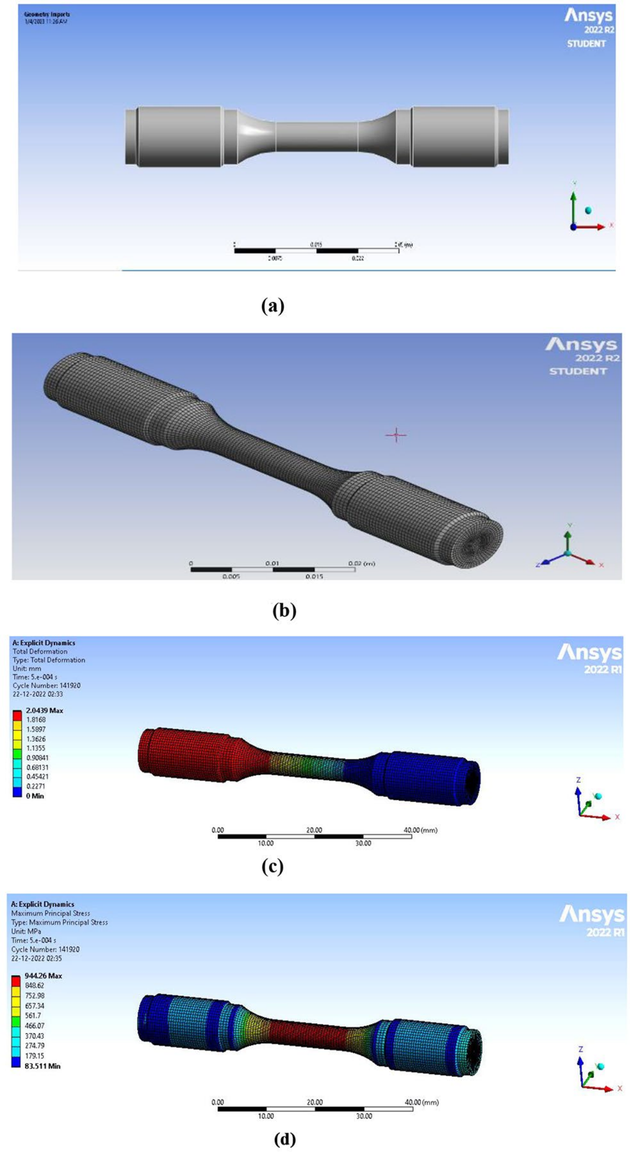

Fig. 7 **(a)** Geometric model, **(b)** Meshed model, **(c)** Equivalent stress, **(d)** Maximum principle stress

3.4 Numerical simulation

The geometric model of the tensile test sample (Fig. 2(b)) is created in ANSYS workbench 22 as shown in Fig. 7a, the discretized model of geometric model is presented in Fig. 7b. It consists of 92,092 nodes & 88,040 Hexa elements the finite element simulations of tensile test were conducted using dynamic explicit formulation. Finite element analysis is performed using some amount of the experimental data for boundary & initial conditions. Commonly used Inconel 718 superalloys elastic properties were assumed, including a young's modulus of 210 GPa & Poisson ratio of 0.3. The output of the FE model such as total deformation, equivalent stress & maximum principle stress (as shown in Fig. 7c, d and e) for different condition are compared & validated with specific experimental results values as tabulated in Table 3.

3.5 Tensile fractured specimen observations

Figure 8 shows the overall fracture surfaces of the IN718 specimens after uniaxial tensile testing at room temperature(RT) and 800 °C.The following results of the fracture surface of the tensile test are obtained using a scanning electron microscope (SEM) at X500 magnification:

After a tensile test at RT, the specimen's fractograph is shown in Fig. 8a. A ductile transgranular fracture mode occurred, according to the many equiaxed dimples present on the fracture surface [15–21]. On the surface, a few distinct voids can also be seen.After a tensile test at RT, the specimen's fractograph is shown in Fig. 8a. The fracture surface's abundance of equiaxed dimples suggests that a ductile transgranular fracture mode took place. On the surface, a few distinct cavities can also be seen [22–31]. A sample that has been induction hardened (IHT1) has shallow dimple voids and fractures in a ductile, transgranular manner at room temperature (Fig. 8c), but the sample fractured in an intergranular, brittle manner at 800 °C (Fig. 8d). Figure 8e of the finding for induction hardening IHT2 at RT shows features that are substantially comparable to those of IHT1 at RT [32–40]. It exhibits ductile brittle transgranular fracture mode as well, but carbide particles are dispersed over the void walls. Transgranular brittle fracture was visible

Table 3 Numerical results of untreated and induction hardened at room temperature and at elevated temperature (800°C)

Tested Specimen	TotalDeformation (mm)	Equivalent Stress (MPa)	Maximum Principle Stress (MPa)
NR_RT	2.0439	931.7	944.26
NR_ET	0.10071	620.55	697.36
IHT1_RT	0.1728	1065.1	1234.78
IHT1_ET	0.10143	624.98	713.67
IHT2_RT	0.1973	1216.2	1424.68
IHT2_ET	0.1158	713.55	817.58

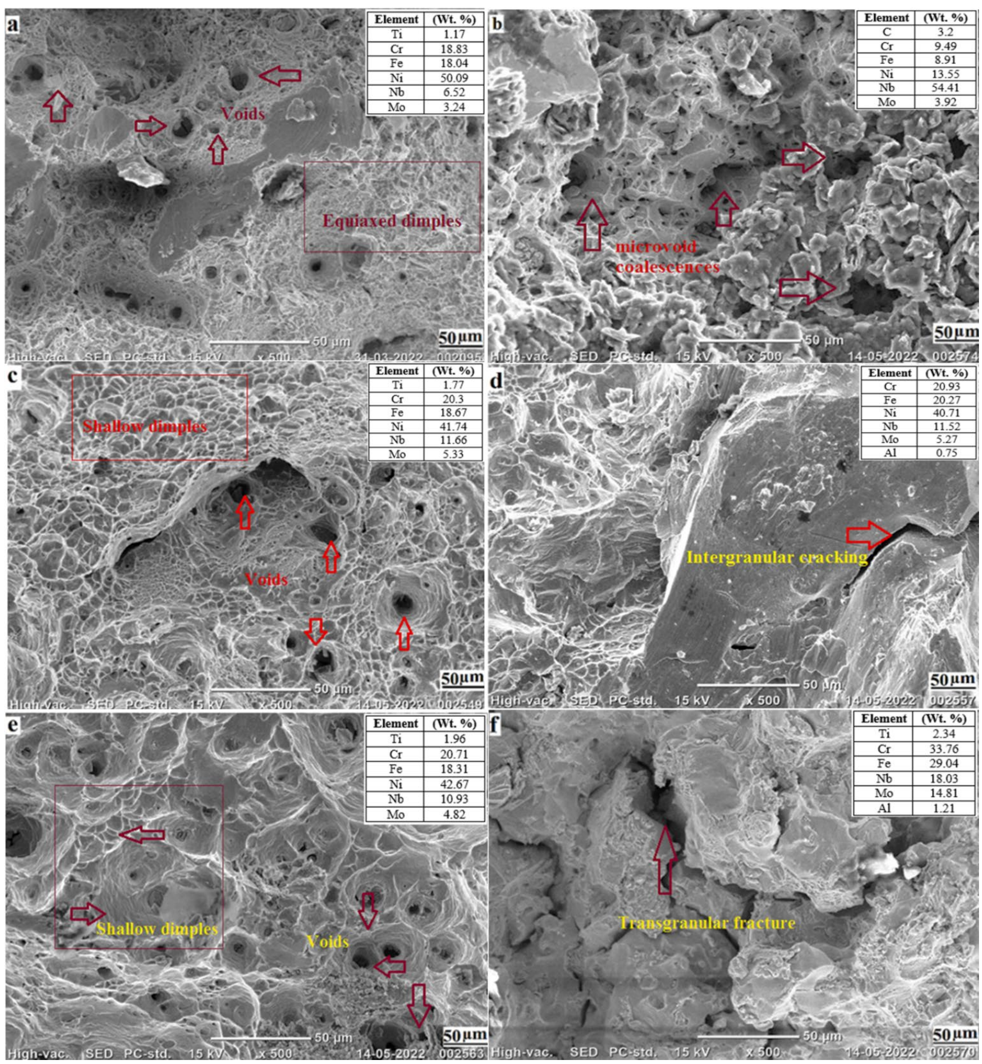

Fig. 8 Fractography of IN718 of untreated and induction hardened samples at room and elevated temperature **(a)** untreated sample at room tempeature **(b)** untreated sample at elevated temperature **(c)** IHT1 sample at room tempeature **(d)** IHT1 sample at elevated temperature **(e)** IHT2 sample at room tempeature **(f)** IHT2 sample at elevated temperature

during induction hardening of IHT2 at a high temperature of 800 °C (Fig. 8f) [6]. Based on the abundant equiaxed dimples on the fracture surface (Fig. 8a, c), it can be said that the fracture mechanism is a typical transgranular ductile fracture at room temperature (RT). At 800 °C, however, the fracture is covered with numerous shallow dimples and intergranular cracks, indicating a predominately intergranular brittle fracture with a minor amount of ductile fracture (Fig. 8b, d, f). This transition from transgranular to intergranular fracture is the impact to the decrease of strength and ductility [43–49].

Energy dispersive X-ray spectroscopy (EDS) analysis is used to verify that the chemical elements of the microstructure. The analysis shows how the chemical constituents vary along a line that cuts across the matrix phase field, the carbide veins and the scattered phase. Figure 8a and f demonstrate that nickel, one of the components responsible for the creation of both phases, is substantially more abundant in the γ and $\gamma^{'}$ phase than it is in the carbides [50–58]. Niobium, molybdenum, titanium, and iron are the elements that are primarily found in carbides. Niobium concentration decreased in the matrix phase with induction hardening, and increasing its relative concentration to other elements like molybdenum, titanium and iron [59–65].

4 Conclusion

Primarily the induction hardening of IN718 superalloy (IHT1 & IHT2) at 850^0 C & 1000^0 C with oil quenching is done. The tensile strength behavior of untreated, induction hardened IHT1 & IHT2 were assented at room temperature & elevated temperature of 800^0 C.

Main finding of the present studies are as follows:

- In the induction hardened at T = 1000℃ (IHT2) it can be observed that the grains are equiaxed with the equal grain size.
- The existence of the γ'' and γ' phases shows that the specimens' plasticity increases with induction hardening [23 & 28].
- In case of elevated temperature (800^0 C) of IHT1 & IHT2 large amount of intergranular cracks are observed on surface & the fracture microstructure are characterised by lots shallow dimples which reveals a combination of transgranular & intergranular fracture mode.
- The tensile test numericalresults obtained from ANSYS workbench are validated with experimental values and proved that induction hardenedsamples has better mechanical properties in comparison to non-induction hardened samples.
- The obtained results will be further used to study fatigue life of induction hardened IN718.

Acknowledgements We would like to thanks the Visvesvarya Technology University (VTU) regional research center, Department of Mechanical Engineering, RV college of Engineering Bengaluru, Karnataka-india for providing facilities to conduct this research work.

Declarations

Competing interests This article has not been submitted elsewhere for publication and authors do not have any conflict related to this manuscript and presented data.

References

1. Hitesh Vasudev, L., Thakur, A., Bansal, H., Singh, Zafar, S.: *"High temperature oxidation and erosion behaviour of HVOF sprayed bi-layer Alloy-718/NiCrAlY coating"*, Surface and Coatings Technology,362 pp.366–380. (2019)
2. Prashar, G., Vasudev, H.: Surface topology analysis of plasma sprayed Inconel625-Al2O3 composite coating," Materials Today: Proceedings, no. xxxx, 2021(Elsevier, Scopus Indexed). Volume 50, Part 5, Pages 607–611 (2022). https://doi.org/10.1016/j.matpr.2021.03.090
3. Hitesh Vasudev, P., Singh, L., Thakur, Bansal, A.: "Mechanical and microstructural characterization of microwave post processed Alloy-718 coating," *Materials Research Express*, vol. 6, no. 12, p. 1265f5, Jan. (2020)
4. Hitesh Vasudev, L., Thakur, A., Bansal, H., Singh: *An investigation on oxidation behaviour of high velocity oxy-fuel sprayed IN718- Al_2O_3composite coatings*. Surf. Coat. Technol. (2020). https://doi.org/10.1016/j.surfcoat.2020.125770
5. Vasudev, H., Thakur, L., Singh, H., Bansal, A.: A study on processing and hot corrosion behaviour of HVOF sprayed Inconel718-nano Al_2O_3 coatings. Mater. Today Commun. **25**, 101626 (2020). https://doi.org/10.1016/j.mtcomm.2020.101626
6. Vasudev, H., Prashar, G., Thakur, L.: and A. Bansal, "Microstructural characterization and electrochemical corrosion behaviour of HVOF sprayed Alloy718-nanoAl_2O_3 composite coatings", *Surface Topography: Metrology and Properties* 9 10.1088/2051-672X/ac1044 (2021)
7. Vasudev, H., Thakur, L., Bansal, A., Singh, H.: Erosion behaviour of HVOF sprayed Alloy718-nano Al_2O_3 composite coatings on grey cast iron at elevated temperature conditions. Surf. Topogr. Metrol. Prop. (2021). https://doi.org/10.1088/2051-672X/ac1c80
8. Vasudev, H., Prashar, G., Thakur, L., Bansal, A.: "Electrochemical Corrosion Behaviour and Microstructural Characterization of HVOF Sprayed Inconel718-Al_2O_3 Composite Coatings" *Surface review and letters*; (2021). https://doi.org/10.1142/S0218625X22500172
9. WANG, Y., SHAO, W.Z., YANG, Z.H.E.N.L., ZHANG, C. XM: Tensile deformation behavior of superalloy 718 at elevated temperatures. J. Alloys Compd. **471**, 331–335 (2009). https://doi.org/10.1016/j.jallcom.2008.03.082
10. LIU, B.B., HAN, J.Q., ZHAO, R., LIU, W., WAN, M.: Grain size effect on fracture behavior of the axis-tensile test of Inconel 718 sheet. High. Temp. Mater. Proc. **35**, 989–998 (2016). https://doi.org/10.1515/htmp-2015-0102
11. ZHAO, R., LI, X.J., WAN, M., HAN, J.Q., MENG, B., CAI, Z.Y.: Fracture behavior of Inconel 718 sheet in thermal-aideddeformation considering grain size effect and strain rate influence.

Mater. Des. **130**, 413–425 (2017). https://doi.org/10.1016/j.matdes.2017.05.089
12. LIN, Y.C., DENG, J., JIANG, Y.Q., WEN, D.X., LIU, G.: Hot tensile deformation behaviors and fracture characteristics of a typical Ni-based superalloy. Mater. Des. **55**, 949–957 (2014). https://doi.org/10.1016/j.matdes.2013.10.071
13. Sharma, Y., K.Singh and, Vasudev, H.: Experimental studies on friction stir welding of aluminium alloys," *Materials Today: Proceedings*, Volume 50, Part 5, Pages 2387–2391 (2022). https://doi.org/10.1016/j.matpr.2021.10.254
14. Singh, G., Vasudev, H., Bansal, A.: Influence of heat treatment on the microstructure and corrosion properties of the Inconel-625 clad deposited by microwave heating. Surf. Topogr. Metrol. Prop. **9**, 025019 (2021). https://doi.org/10.1088/2051-672X/abfc61
15. Amit Bansal, H., Vasudev, P., kumar, A.K., Sharma: Investigation on the effect of post weld heat treatment on microwave joining of the Alloy-718 weldment. Mater. Res. Express. **8**, 1–12 (2019)
16. DU, B., YANG, J., CUI, C., SUN, X.: Effects of grain refinement on the microstructure and tensile behavior of K417G superalloy. Mater. Sci. Eng. A. **623**, 59–67 (2015). https://doi.org/10.1016/j.msea.2014.11.041
17. LIN, Y.C., LI, L., HE, D.G., CHEN, M.S., LIU, G.Q.: Effects of pre-treatments on mechanical properties and fracture mechanism of a nickel-based superalloy. Mater. Sci. Eng. A. **679**, 401–409 (2017). https://doi.org/10.1016/j.msea.2016.10.058
18. LIN, Y.C., DENG, J., JIANG, Y.Q., WEN, D.X., LIU, G.: Hot tensile deformation behaviors and fracture characteristics of a typical Ni-based superalloy. *Mater Des* 55:949–957. https://doi/org/j.matdes.2013.10.071. (2014)
19. ZHAO, R., LI, X.J., WAN, M., HAN, J.Q., MENG, B., CAI, Z.Y.: Fracture behavior of Inconel 718 sheet in thermal-aided deformation considering grain size effect and strain rate influence. Mater. Des. **130**, 413–425 (2017). https://doi.org/10.1016/j.matdes.2017.05.089
20. LIU, Z.G., LI, P.J., XIONG, L.T., LIU, T.Y., HE, L.J.: High temperature tensile deformation behavior and microstructure evolution of Ti55 titanium alloy. Mater. Sci. EngA. **680**, 259–269 (2017). https://doi.org/10.1016/j.msea.2016.10.095
21. LI, X.F., ZHANG, J., FU, Q.Q., SONG, A.K.I.Y.A.M.A.E., WANG, X.L., LI, Y.F., ZOU, Q.Z. N: Tensile mechanical properties and fracture behaviors of nickel-based superalloy 718 in the presence of hydrogen. Int. J. Hydrog Energy. **43**, 20118–20132 (2018). https://doi.org/10.1016/j.ihydene.2018.08.179
22. ALABORT, E., BARBA, D., SULZER, S., LIBNER, M., PETRINIC, N., REED, R.C.: Grain boundary properties of a nickel-based superalloy: Characterisation and modeling. Acta Mater. **151**, 377–394 (2018). https://doi.org/10.1016/jactamat.2018.03.059
23. ZHANG, Z.Y.U.J., YUAN, Y., ZHOU, R., ZHANG, H., WANG, H.: Microstructural evolution and mechanical properties of Inconel 718 after thermal exposure. Mater. Sci. Eng. A. **634**, 55–63 (2015). https://doi.org/10.1016/j.msea.2015.03.004
24. ZHANG, L., LI, D., QU, X.H., QIN, M.L., HE, X.B., LI, Z.: Microstructure and tensile properties optimization of MIM418 superalloy by heat treatment. J. Mater. Process. Technol. **227**, 71–79 (2016). https://doi.org/10.1016/j.jmatprotec.2015.08.001
25. OZGUN, O., YILMAZ, R., GULSOY, H.O., FINDIK, F.: The effect of aging treatment on the fracture toughness and impact strength of injection molded Ni-625 superalloy parts. Mater. Charact. **108**, 8–15 (2015). https://doi.org/10.1016/j.matchar.2015.08
26. Sudheer, D., Kulkarni, M., Chandrasekhar, U., Manjunath, K.V., Durga Prasad, C., Vasudev, H.: "Design and Optimization of Polyvinyl-Nitride Rubber for Tensile Strength Analysis", *International Journal on Interactive Design and Manufacturing (IJIDeM)*, Springer, (2023). https://doi.org/10.1007/s12008-023-01405-6
27. Mahantesh, M., Math, Rajeswara Rao, K.V.S., Prapul Chandra, A.C., Vijayakumar, M.N., Nandini, B., Prasad, C.D., Vasudev, H.: "Design and Modeling using Finite Element Analysis for the Sitting Posture of Computer Users Based on Ergonomic Perspective", *International Journal on Interactive Design and Manufacturing (IJIDeM)*, Springer, (2023). https://doi.org/10.1007/s12008-023-01383-9
28. Madhu Sudana Reddy, G., Durga Prasad, C., Kollur, S., Lakshmikanthan, A., Suresh, R.: Aprameya C R, "Investigation of High Temperature Erosion Behaviour of NiCrAlY/TiO2 Plasma Coatings on Titanium Substrate", *JOM The Journal of The Minerals, Metals & Materials* Society *(TMS)*, Springer, https://doi.org/10.1007/s11837-023-05894-4
29. Pulla Nagabhushana, S., Ramprasad, C.D., Prasad, H., Vasudev, C., Prakash: "Numerical Investigation on Heat Transfer of a Nano-Fluid Saturated Vertical Composite Porous Channel Packed between Two Fluid Layers", *International Journal on Interactive Design and Manufacturing (IJIDeM)*, Springer, (2023). https://doi.org/10.1007/s12008-023-01379-5
30. Praveen, N., Mallik, U.S., Shivasiddaramaih, A.G., Suresh, R., Durga Prasad, C., Shivaramu, L.: "Synthesis and Wire EDM Characteristics of Cu–Al–Mn Ternary Shape Memory Alloys Using Taguchi Method", *Journal of The Institution of Engineers (India): Series D*, Springer, (2023). https://doi.org/10.1007/s40033-023-00501-x
31. Anjaneya, G., Sunil, S., Kakkeri, S., Mahantesh, M., Math, M.N., Vaibhav, C., Solaimuthu, C.D., Prasad, H., Vasudev: "Numerical Simulation of Microchannel Heat Exchanger using CFD", *International Journal on Interactive Design and Manufacturing (IJIDeM)*, Springer, (2023). https://doi.org/10.1007/s12008-023-01376-8
32. Mohan Poojari, H., Hanumanthappa, C.D., Prasad, H.M., Jathanna, A.R., Ksheerasagar, P., Shetty, B.K., Shanmugam, H., Vasudev: "Computational Modelling for the Manufacturing of Solar-Powered Multifunctional Agricultural Robot", *International Journal on Interactive Design and Manufacturing (IJIDeM)*, Springer, (2023). https://doi.org/10.1007/s12008-023-01291-y
33. Manjunatha, C.J., Durga Prasad, C., Harish Hanumanthappa, R., Kannan, A., Dhanesh, G., Mohan, B.K., Shanmugam, Venkategowda, C.: "Influence of Microstructural Characteristics on Wear and Corrosion Behaviour of Si_3N_4 Reinforced Al2219 Composites", *Advances in Materials Science and Engineering*, Hindawi, vol. Article ID 1120569, (2023), (2023). https://doi.org/10.1155/2023/1120569
34. Sharanabasva, H., Durga Prasad, C.: Characterization and wear behavior of NiCrMoSi Microwave Cladding. J. Mater. Eng. Perform. (2023). https://doi.org/10.1007/s11665-023-07998-z
35. Sharanabasva, H., Durga Prasad, C.: Effect of Mo and SiC reinforced NiCr Microwave Cladding on microstructure, mechanical and wear Properties. J. Institution Eng. (India): Ser. D. (2023). https://doi.org/10.1007/s40033-022-00445-8
36. Nithin, H.S., Nishchitha, K.M., Pradeep, D.G., Durga Prasad, C., Mathapati, M.: Comparative analysis of CoCrAlY Coatings at High Temperature Oxidation Behavior using different reinforcement composition profiles. Weld. World. **67**, 585–592 (2023). https://doi.org/10.1007/s40194-022-01405-2
37. Naveen, D.C., Naresh Kakur, Keerthi Gowda, B.S., Madhu Sudana Reddy, G., Durga Prasad, C., Ragavanantham Shanmugam: "Effects of Polypropylene Waste Addition as Coarse Aggregate in Concrete: Experimental Characterization and Statistical Analysis", *Advances in Materials Science and Engineering*, Hindawi, vol. Article ID 7886722, 11 pages, (2022), (2022). https://doi.org/10.1155/2022/7886722
38. Venkate Gowda, H., Hanumanthappa, B.K., Shanmugam, C., Durga Prasad, T.N., Sreenivasa, M.S., Rajendra Kumar: High-temperature Tribological Studies on Hot Forged Al6061- Tib_2

In-Situ Composites. J. Bio Tribo-Corrosion. **8**, 101 (2022). https://doi.org/10.1007/s40735-022-00699-5

39. Madhusudana Reddy, G., Durga Prasad, C., Patil, P., Kakur, N., Ramesh, M.R.: Elevated temperature Erosion performance of plasma sprayed NiCrAlY/TiO_2 coating on MDN 420 Steel substrate. Surf. Topogr. Metrol. Prop. **10**, 025010 (2022). https://doi.org/10.1088/2051-672X/ac6a6e
40. Madhusudana Reddy, G., Durga Prasad, C., Shetty, G., Nageswara Rao, R.M.R. T, and, Patil, P.: "Investigation of thermally sprayed NiCrAlY/TiO_2 and NiCrAlY/Cr_2O_3/YSZ Cermet Composite Coatings on Titanium Alloys". Eng. Res. Express, Vol **4**, 025049, https://doi.org/10.1088/2631-8695/ac7946
41. Madhusudana Reddy, G., Durga Prasad, C., Shetty, G., Nageswara Rao, R.M.R. T and, Patil, P.: "High Temperature Oxidation Behavior of Plasma Sprayed NiCrAlY/TiO_2 & NiCrAlY /Cr_2O_3/YSZ Coatings on Titanium Alloy". *Welding in the World, Springer* (2022). https://doi.org/10.1007/s40194-022-01268-7
42. Thavaraya Naik, M., Mathapathi, C., Durga Prasad, Nithin, H.S., Ramesh, M.R.: Effect of laser Post Treatment on Microstructural and sliding wear behavior of HVOF sprayed NiCrC and NiCrSi Coatings. Surf. Rev. Lett. **29**(1), 225000 (2022). https://doi.org/10.1142/S0218625X2250007X
43. Madhusudana Reddy, G., Durga Prasad, C., Shetty, G., Nageswara Rao, R.M.R. T and, Patil, P.: High temperature oxidation studies of plasma sprayed NiCrAlY/TiO_2 & NiCrAlY /Cr_2O_3/YSZ Cermet Composite Coatings on MDN-420 Special Steel Alloy. Metallography Microstruct. Anal. **10**, 642–651 (2021). https://doi.org/10.1007/s13632-021-00784-0
44. Mahantayya Mathapati, K., Amate, C., Durga Prasad, Jayavardhana, M.L., Hemanth Raju, T.: "A Review on Fly ash Utilization". *Materials Today Proceedings, Elsevier Science*, Vol. 50, Part 5, pp 1535–1540. (2022). https://doi.org/10.1016/j.matpr.2021.09.106
45. Rayirth Dinesh, Rohan Raykar, S., Rakesh, T.L., Prajwal, M.G., Shashank Lingappa, M., Durga Prasad, C.: "Feasibility study on MoCoCrSi/ WC-Co cladding developed on austenitic stainless steel using microwave hybrid heating". J. Mines Met. Fuels, Volume 69, Issue 12A, December 2021, https://doi.org/10.18311/jmmf/2021/30113
46. Prasad, C.D., Lingappa, S., Joladarashi, S., Ramesh, M.R., Sachin, B.: "Characterization and Sliding Wear Behavior of CoMoCrSi + Flyash Composite Cladding Processed by Microwave irradiation", *Materials Today Proceedings, Elsevier Science*, vol 46, pp 2387–2391, (2021). https://doi.org/10.1016/j.matpr.2021.01.156
47. Madhu, G., Mrityunjaya Swamy, K.M., Kumar, D.A., Durga Prasad, C., Harish, U.: Evaluation of hot corrosion behavior of HVOF thermally sprayed Cr_3C_2 -35NiCr coating on SS 304 boiler tube steel. Am. Inst. Phys. **2316**, 030014 (2021). https://doi.org/10.1063/5.0038279
48. Prasad, C.D., Mathapathi, M., Vasudev, H., Thakur, L.: "Analysis of Mechanical Properties and Microstructural Characterisation of Microwave Cladding on Stainless Steel", in a book titled "*Advances in Microwave Processing for Engineering Materials*", CRC Press, Taylor & Francis Group, ISBN: 9781003248743, (2022). https://doi.org/10.1201/9781003248743
49. Prasad, C.D., Mathapathi, M., Joladarashi, S., Ramesh, M.R., Francis Group: "Investigation of Microstructural and Tribological Behavior of Metco 41 C + WC-12Co Composite Coating Sprayed by HVOF Process", in a book titled "*Thermal Spray Coatings*". CRC Press, Taylor and. ISBN: 9781032081489. (2021). https://doi.org/10.1201/9781003213185
50. Prasad, C.D., Jerri, A., Ramesh, M.R., Francis Group: "Evaluation of Microstructural and Dry Sliding Wear Resistance of Iron-Based SiC-Reinforced Composite Coating by HVOF Process", in a book titled "*Thermal Spray Coatings*". CRC Press, Taylor and. ISBN: 9781032081489. (2021). https://doi.org/10.1201/9781003213185
51. Sachin, B., Charitha, M., Rao, G.M., Naik, D., Prasad, C., Ajit, M., Hebbale, Vijeesh, V., Muralidhara Rao: "Minimum quantity lubrication and cryogenic for burnishing of difficult to cut material as a sustainable alternative", Lecture Notes in Mechanical Engineering. Springer, ISBN - 978-981-16-2278-6, (2021). https://doi.org/10.1007/978-981-16-2278-6_6
52. Reddy, M.S., Durga Prasad, C., Patil, P., Ramesh, M.R., Rao, N.: Hot corrosion behavior of plasma sprayed NiCrAlY/TiO_2 and NiCrAlY/Cr_2O_3/YSZ cermets coatings on alloy steel. Surf. Interfaces Elsevier Sci. **22**, 100810 (2021). https://doi.org/10.1016/j.surfin.2020.100810
53. Prasad, C.D., Joladarashi, S., Ramesh, M.R., Srinath, M.S.: Microstructure and Tribological Resistance of Flame sprayed CoMoCrSi/WC-CrC-Ni and CoMoCrSi/WC-12Co composite Coatings Remelted by Microwave Hybrid Heating. J. Bio Tribo-Corrosion Springer. **6**, 124 (2020). https://doi.org/10.1007/s40735-020-00421-3
54. Durga Prasad, C., Joladarashi, S., Ramesh, M.R.: Comparative investigation of HVOF and Flame Sprayed CoMoCrSi Coating. Am. Inst. Phys. **2247**, 050004 (2020). https://doi.org/10.1063/5.0003883
55. Prasad, C.D., Jerri, A., Ramesh, M.R.: Characterization and sliding wear behavior of Iron Based Metallic Coating deposited by HVOF process on low Carbon Steel substrate. J. Bio Tribo-Corrosion Springer. **6**, 69 (2020). https://doi.org/10.1007/s40735-020-00366-7
56. Prasad, C.D., Joladarashi, S., Ramesh, M.R., Srinath, M.S., Channabasappa, B.H.: "Comparison of High Temperature Wear Behavior of Microwave Assisted HVOF Sprayed CoMoCrSi-WC-CrC-Ni/WC-12Co Composite Coatings". *Silicon, Springer*, 12, pp 3027–3045 1–19 (2020). https://doi.org/10.1007/s12633-020-00398-1
57. Giridhar, S., Kulkarni, N.G., Siddeshkumar, C., Durga Prasad, L., Shankar, Suresh, R.: "Drilling of GFRP with Liquid Silicon Rubber Reinforced with fine Aluminium Powder on Hole Surface Quality and Tool Wear using DOE", *Journal of Bio- and Tribo-Corrosion*, Springer, volume 9, Article number: 53 (2023). https://doi.org/10.1007/s40735-023-00771-8
58. Durga Prasad, C., Joladarashi, S., Ramesh, M.R., Srinath, M.S., Channabasappa, B.H.: Effect of microwave heating on microstructure and elevated temperature Adhesive wear behavior of HVOF deposited CoMoCrSi-Cr_3C_2 Composite Coating. Surf. Coat. Technol. Elsevier Sci. **374**, 291–304 (2019). https://doi.org/10.1016/j.surfcoat.2019.05.056
59. Prasad, C.D., Joladarashi, S., Ramesh, M.R., Srinath, M.S., Channabasappa, B.H.: Development and sliding wear behavior of Co-Mo-Cr-Si Cladding through Microwave Heating. Silicon, Springer. **11**, 2975–2986 (2019). https://doi.org/10.1007/s12633-019-0084-5
60. Prasad, C.D., Joladarashi, S., Ramesh, M.R., Srinath, M.S., Channabasappa, B.H.: Microstructure and Tribological Behavior of Flame Sprayed and Microwave Fused CoMoCrSi/CoMoCrSi-Cr_3C_2 Coatings. Mater. Res. Express. **6**, 026512 (2019). https://doi.org/10.1088/2053-1591/aaebd9
61. Prasad, C.D., Joladarashi, S., Ramesh, M.R., Srinath, M.S., Channabasappa, B.H.: Influence of microwave hybrid heating on the sliding wear behaviour of HVOF sprayed CoMoCrSi Coating. Mater. Res. Express. **5**, 086519 (2018). https://doi.org/10.1088/2053-1591/aad44e
62. Durga Prasad, C., Joladarashi, S., Ramesh, M.R.: Anunoy Sarkar. "High Temperature Gradient Cobalt based Clad Developed Using Microwave Hybrid Heating". *American Institute of Physics*, 1943, 020111 (2018). https://doi.org/10.1063/1.5029687

63. Girisha, K.G., Sreenivas Rao, K.V., Prasad, D.: C, "Slurry Erosion Resistance of Martenistic Stainless Steel with Plasma Sprayed Al_2O_3-40%TiO_2 Coatings", *Materials Today Proceedings* 5 7388–7393. (2018). https://doi.org/10.1016/j.matpr.2017.11.409
64. Girisha, K.G., Durga Prasad, C., Anil, K.C., Sreenivas Rao, K.V.: Dry sliding wear behaviour of Al2O3 coatings for AISI 410 grade stainless steel. Appl. Mech. Mater. **766–767**, 585–589 (2015). https://doi.org/10.4028/www.scientific.net/AMM.766-767.585
65. Girisha, K.G., Rakesh, R., Durga Prasad, C., Sreenivas Rao, K.V.: Development of corrosion resistance coating for AISI 410 grade steel. Appl. Mech. Mater. **813–814**, 135–139 (2015). https://doi.org/10.4028/www.scientific.net/AMM.813-814.135